Optics Communications 501 (2021) 127377

Contents lists available at ScienceDirect

Optics Communications

journal homepage: www.elsevier.com/locate/optcom

Multi-element full-duplex FSO transceiver design using optimum tiling

A.F.M. Saniul Haq [a,*], Murat Yuksel [a,b]

[a] CREOL, The College of Optics and Photonics, University of Central Florida, FL, 32816, USA
[b] The Department of Electrical and Computer Engineering, University of Central Florida, FL, 32816, USA

ARTICLE INFO

Keywords:
Optical wireless communication
In-band full-duplex (IBFD)
Free space optics
Transceiver design
Multi-element tiling

ABSTRACT

With ever-growing demand of high-speed mobile data and in vision of smart cities, optical wireless, a.k.a. free-space optical (FSO), communication deem to be a critical technology due to its significantly faster data transfer rate, higher security, lower costs, and reduced power usage. These beneficial effects have led to interest in exploring FSO technologies for mobile platforms such as drone-based cell tower to provide Internet services to remote areas, or even for wireless communications on the ground with jammed radio channels as in battlefields. Direct line-of-sight (LOS) is required to establish secure directional FSO communication (FSOC) links which are highly susceptible to random and erratic movements of the mobile nodes as well as the turbulence in the free-space medium. The performance of FSOC links can be improved by designing multi-element tiling of the laser-based transceivers which is capable of in-band full-duplex (IBFD) communication. In this work, we propose a genetic algorithm framework to explore optimized multi-element FSO transceiver tiling patterns to ensure maximal signal-to-interference and noise ratio (SINR) and minimize the effects of vibration of the mobile platform and atmospheric turbulence.

1. Introduction

Increase in mobility and number of users triggered a sharp increase in wireless data demands for communication devices, sensor networks, and security protocols. The ever-increasing data demand for smartphones, peer-to-peer networks, and autonomous vehicles are over-crowding the legacy radio-frequency (RF) bands below 6 GHz and in immediate need of alternative bands, such as optical and millimeter wave (mmWave). High speed wireless networks for mobile applications use mostly RF-based Wi-Fi points nowadays, but the bandwidth and capacity mismatch with the fiber optical backhaul network cannot deliver full potential of the system, which can be achieved by complementing, and in some cases replacing with free-space optical (FSO) networks [1–3].

FSO communication (FSOC) can enable high speed mobile ad hoc network for futuristic smart city implementations because of the high modulation speed, higher bandwidth, unlicensed spectrum, and secure directional beam propagation. The use of light emitting diodes (LEDs) and lasers for communication may ensure low cost, low power, dense packaging, and systems for high speed communication between mobile and/or fixed nodes. Low divergence angle and moderate field-of-view (FOV) of the optical components lead to spatial reuse, multiple channels, and a multi-node system to reach wider range of coverage. However, direct line-of-sight (LOS) and weather-dependent beam propagation loss limit the applications of FSOC to indoor and short range (~100 m) outdoor applications.

Mobile FSO networks can be a useful solution for multi-node, high speed, and short distance communication. Tactical ad hoc networks with requirement of high bandwidth and reduced probability of jamming and interception can greatly benefit from implementing nodes with FSO transceivers. Beyond these advantages, the network capacity can be significantly increased by utilizing the FSO transceivers in an in-band full-duplex (IBFD) manner. IBFD communication uses simultaneous signal transmission and reception in the same frequency band. Despite the disadvantages caused by self-interference (SI), full-duplex operation can aid in successfully dealing with the huge spectrum demands by increased channel capacity.

Some of the drawbacks of IBFD FSOC can be addressed implementing multi-element transceiver nodes with capability of spatial reuse, beam steering, cognitive techniques for adaptive optimizations, and tolerance to mobility, vibration, sway, or tilt during communication. The single most *key limitation of the mobile FSOC is to maintain the link under perturbation*. The alignment of the transmitter and receiver might need to be compensated for vibration, sway, or tilt to ensure LOS. Intelligent design of a multi-element transceiver plane layout may minimize these loss components and maximize signal-to-interference-plus-noise ratio (SINR) for mobile FSOC links. Moreover, by using solid-state laser arrays, e.g. VCSEL arrays, power consumption and signal strength of the system can be controlled and implemented in various applications, such as LiDAR devices, communication modules, and sensing modules.

* Corresponding author.
E-mail address: saniul.haq@knights.ucf.edu (A.F.M.S. Haq).

https://doi.org/10.1016/j.optcom.2021.127377
Received 22 December 2020; Received in revised form 19 July 2021; Accepted 15 August 2021
Available online 18 August 2021

In this paper, we will address the design and tiling of different elements, i.e., transmitters and receivers, on the transceiver plane to optimize IBFD communication throughput. We explore optimization techniques to find the optimum number of transmitters and tiling those in a fashion that gives uninterrupted performance even in the presence of vibration. The main contributions in this paper are as follows:

- An analytical model of link performance parameter, SINR, is developed for multi-element full-duplex FSO transceiver by considering free-space attenuation as well as the vibration model of the mobile platform, e.g., an unmanned aerial vehicle (UAV).
- An optimized approach of tiling elements within transceiver plane by evaluating randomly generated sets.
- An optimized approach of tiling elements within transceiver plane by implementing genetic algorithm and evaluating multiple generations of solutions to reach the most favorable tiling pattern.

The rest of the paper is organized as follows: In Section 2, we will present motivation for this work and relevant literature review on multi-element full-duplex FSOC. In Section 3, we discuss beam propagation and FSO channel fading model along with atmospheric turbulence and FSO propagation model. In Section 4, we formulate our optimized transceiver design problem, and in Section 5, we present simulation results for our proposed optimized tiling approach by evaluating randomly generated sets. In Section 6, we discuss the genetic evolution approach to achieve the optimized tiling solution for multi-element full-duplex FSO transceiver.

2. Motivation and literature review

As wireless communication is being adopted by users, autonomous cars, and providing Internet services to remote locations, FSO transceiver antenna design attracted a lot of attention during the last decade. In this section, we discuss the literature that addressed different issues regarding full-duplex and multi-element FSO antenna design.

2.1. Full-duplex FSOC

Even in the presence of self-interference (SI), full-duplex communication can provide at least 20% gain over half-duplex communication [4]. A multi-access control (MAC) protocol for full-duplex radio communication is proposed by Goyal et al. [5] that helps achieve 88% throughput gain. Also, the effect of SI reduces significantly with increase in directionality of the transmitter and the receiver [6]. Prior work on full-duplex FSOC has reported transceiver designs using *out-of-band* techniques. Full-duplex indoor FSOC is demonstrated for error-free ($BER < 10^{-9}$) short range operation [7]. The transceiver used different optical wavelengths for uplink (1550.12 nm) and downlink (850 nm) channels, which makes it an out-of-band design. To suppress the SI for full-duplex operation, two separate bands are used for the transmitter and the receiver. Wang et al. [8] reported a full-duplex visible light communication (VLC) system which implements sub-carrier multiplexing (SCM) and wavelength division multiplexing (WDM) techniques based on commercially available LEDs. Bit-error rate reported for 66 cm free-space delivery was 3.8×10^{-3}, but the use of red–green–blue (RGB) LEDs essentially make the design out-of-band.

IBFD FSOC designs have recently received attention. An IBFD design for FSOC has been reported by Oh et al. [3], which implements communication between a stationary controller and a mobile node using beam reversibility and data erasure method. Even though this design implements full-duplex operation for the mobile node, the controller has only a transmitter but no receiver. Johnson et al. proposed isolating the transmitter and the receiver of a node using a divider, but no functional prototype was demonstrated [9]. In our earlier work [10,11], we demonstrated isolation of infrared transmitter and receiver in an IBFD FSO transceiver for communication among drones. However, these prior studies used LEDs for transmission. In this work, we consider lasers with much narrower divergence angles offering high bandwidth but requiring more careful handling of the LOS link perturbations due to mobility.

2.2. Multi-element transceivers

To improve link quality and provide higher throughput, a large number of transmitters with directional propagation characteristics over same link can be deployed for FSOC, especially to achieve higher aggregated bandwidth and link robustness due to spatial diversity [12]. Bilgi et al. reported that FSO mobile ad-hoc networks (FSO-MANETs) can be designed using optical antennas in spherical shapes, which can achieve angular diversity, spatial reuse, and multi-element incorporation [13]. Alignment and mobility issues of multi-element FSO transceivers were analyzed and modeled by Kaadan et al. [14]. Also, in a similar fashion but with less focus on angular diversity, several issues on multi-element VLC systems are investigated by Eroğlu et al. [15]. In these works, the authors investigated localization and tracking of users, LED assignments, and transmit power control for optimum operation. In a recent work, a Line-of-Sight (LOS) alignment protocol has been employed to tackle the hand-off issue caused by the mobility of the receivers in a room using multi-element VLC link by optimizing link performance [16]. In contrast, in our work, we focus on designing and *tiling multiple elements on a single transceiver plane* so that we can achieve the best performance out of the established FSO link in terms of robustness against mobility.

3. Optical channel fading model

3.1. Channel model

The transmitter modulates data onto the instantaneous intensity of an optical beam. In this paper, we consider intensity modulated direct detection channels using On–Off Keying (OOK), which is widely employed in practical systems. The received photocurrent signal is related to the incident optical power by the detector responsivity R. The received signal y suffers from a fluctuation in signal intensity due to atmospheric turbulence and misalignment, as well as additive noise, and can be well modeled as

$$y = hRx + n + i_S, \tag{1}$$

where x is the transmitted signal intensity, h is the channel state, i_S is the SI signal received at the receiver from its own transmitter, y is the resulting electrical signal, and n is signal-independent additive white Gaussian noise. The system block diagram consists of two nodes, A and B, as presented in Fig. 1. It also shows the signal flow direction at the presence of atmospheric attenuation parameters (α, γ), which will be discussed in details later.

The channel state h models the random attenuation of the propagation channel. In our model, h arises due to three factors: path loss h_l, geometric spread and pointing errors h_p, and atmospheric turbulence h_a. The channel state can then be formulated as

$$h = h_l h_p h_a. \tag{2}$$

Note that h_l is deterministic, and h_p and h_a are random with distributions discussed later. Since the time scales of these fading processes ($\approx 10^{-3} - 10^{-2}$ s) are far larger than the bit interval ($\approx 10^{-9}$ s), h is considered to be constant over a large number of transmitted bits. Notice that the use of interleaving to allow for averaging over a large number of fading states is impractical in this channel. This block fading channel is often termed as slow fading or nonergodic channel in which an h is chosen from the random ensemble according to distribution $f_h(h)$ and fixed over a long block of bits.

3.2. Optical fading model

Optical fading can be attributed to several components of the channel and communication system design. Three major components of optical fading in the channel are atmospheric turbulence, free-space attenuation, and pointing error due to misalignment.

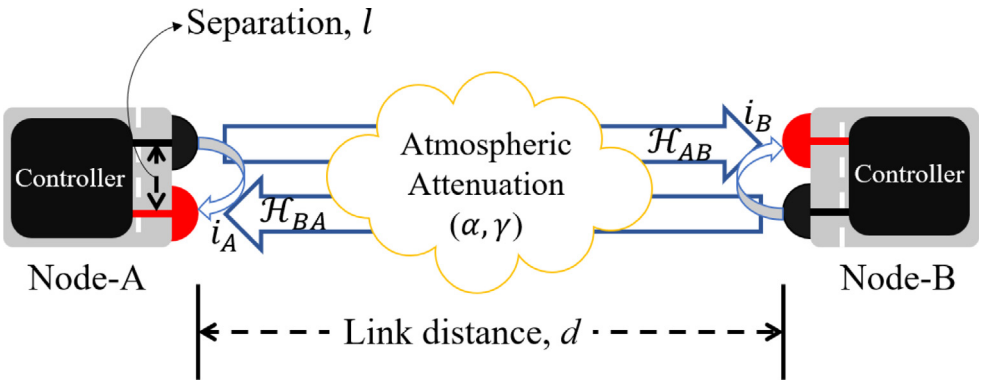

Fig. 1. Block diagram of an in-band full-duplex optical wireless link consisting of two nodes.

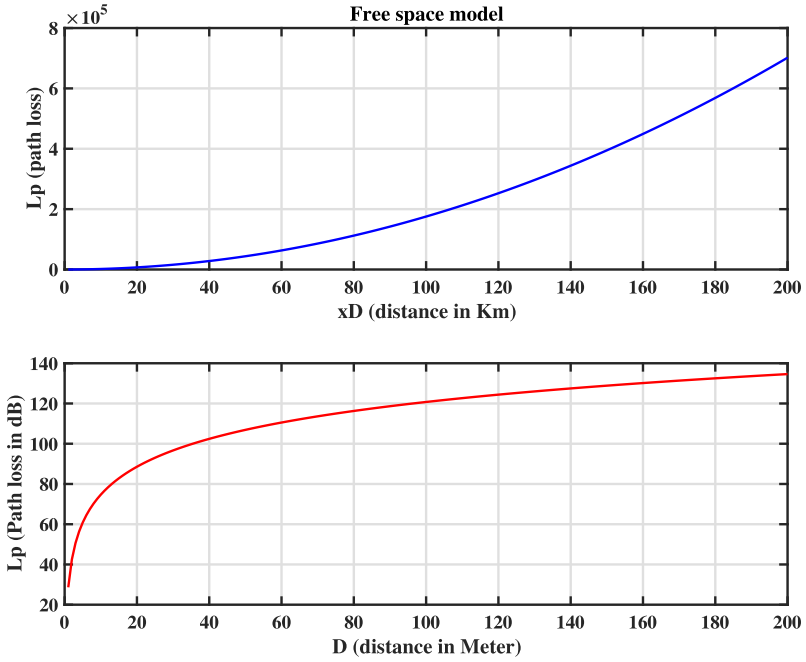

Fig. 2. Path loss calculation for free-space fading model.

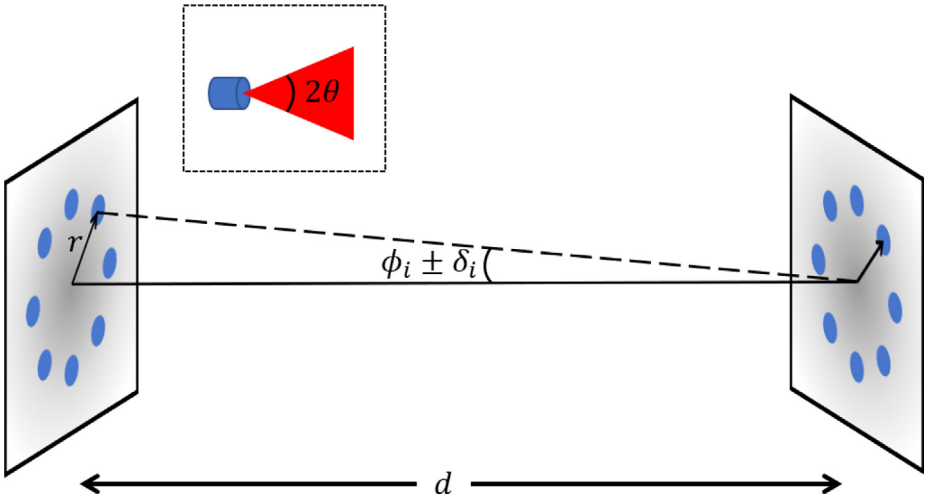

Fig. 3. Orientation of the two communicating nodes after alignment.

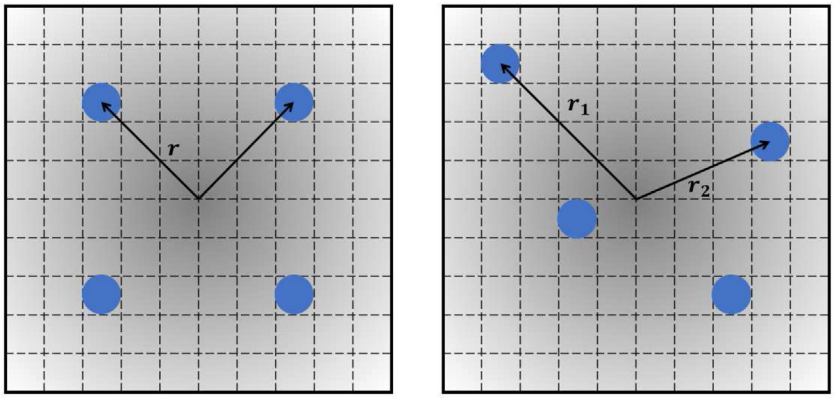

Fig. 4. Position of transmitters within a transceiver plane.

3.2.1. Free-space attenuation

The attenuation of laser power through the atmosphere is described by the exponential Beer–Lambert Law as [17]

$$h_l(z) = \frac{P(z)}{P(0)} = \exp(-\alpha z), \tag{3}$$

where $h_l(z)$ is the loss over a propagation path of length z, $P(z)$ is the laser power at distance z, and α is the attenuation coefficient. The attenuation h_l is considered as a fixed scaling factor during a long period of time, and no randomness exists in its behavior. It depends on the size and distribution of the scattering particles and the wavelength utilized. It can be expressed in terms of the visibility, which can be measured directly from the atmosphere.

By using Friis transmission equation [18], we can calculate the attenuation coefficient as

$$\alpha = \frac{1}{d} \ln \frac{1}{G_T G_R T_A L_{FS}}. \tag{4}$$

The value of α depends on wavelength of the signal λ, visibility range V, and size distribution of the particle q in the atmosphere. The equation of atmospheric attenuation coefficient is proposed by Kim et al. [19] in the form of

$$\alpha = \frac{3.91}{V} \left(\frac{\lambda}{550 \text{ nm}} \right)^{-q}, \tag{5}$$

where q is given by

$$q = \begin{cases} 1.6; & V > 50 \text{ km} \\ 1.3; & 6 \text{ km} < V < 50 \text{ km} \\ 0.72 V^{\frac{1}{3}}; & V < 6 \text{ km}. \end{cases} \tag{6}$$

Using the Eqs. (4)–(6), we have calculated the free-space path loss components with respect to the link distance (d). The loss parameter model (L_p) is shown in Fig. 2.

3.2.2. Pointing error

Loss of LOS or LOS alignment could result in significant channel fading due to pointing error loss. Wind, gust, and thermal expansion of atmospheric medium results in path delay and/or pointing error. We discuss a statistical model to incorporate such pointing error in term of detector aperture, Gaussian beam width, and jitter and vibration variance.

The normalized spatial intensity distribution of the transmitted Gaussian beam is given by [20]

$$I_{beam}(\rho; z) = \frac{2}{\pi w_z^2} \exp\left(-\frac{2\|\rho\|^2}{w_z^2} \right), \tag{7}$$

where ρ is the radial vector from the beam center and w_z is the Gaussian beam waist at distance z, which can be written as

$$w_z \approx w_0 \left[1 + \epsilon \left(\frac{\lambda z}{\pi w_0^2} \right)^2 \right]^{1/2}, \tag{8}$$

where, w_0 is the beam waist at $z = 0$, $\epsilon = (1 + 2w_0^2/\rho_0^2(z))$, and coherent length, $\rho_0(z) = (0.55 C_n^2 k^2 z)^{-3/5}$.

If the center of the incident beam is misaligned by distance r along detector plane, then the fraction of the power collected by the detector, $h_p(.)$, can be expressed as

$$h_p(r; z) = \int_{\mathcal{A}} I_{beam}(\rho - r; z) d\rho, \tag{9}$$

where $\mathcal{A}$ is the area of the detector and h_p is a function of radial misalignment angle when pointing error r is present, as shown in Figs. 3 and 4. Due to symmetry in beam shape and detector area, the integral can be approximated by

$$h_p(r; z) \approx A_0 \exp\left(-\frac{2r^2}{w_{z_{eq}}^2} \right), \tag{10}$$

where

$$A_0 = [\text{erf}(\upsilon)]^2$$

$$w_{z_{eq}}^2 = w_z^2 \frac{\sqrt{\pi}\text{erf}(\upsilon)}{2\upsilon \exp(-\upsilon^2)}$$

$$\upsilon = \frac{\sqrt{\pi} a}{\sqrt{2} w_z},$$

and a is the radius of a single receiver.

4. IBFD FSOC link: SINR formulation

4.1. Noise and self-interference

The noise components when an optical signal is received by the detector consist of various noise sources like Johnson (thermal) noise, background radiation, and dark current. The equations for the noise equivalent power (NEP) of the optical components are given by [21]

$$P_{bg\_sn} = \frac{\sqrt{2qSP_{bg}B_{en}F}}{S}, \tag{11}$$

$$P_{sig\_sn} = \frac{\sqrt{2qSP_{sig}B_{en}F}}{S}, \tag{12}$$

$$P_{dark\_sn} = \frac{\sqrt{\left(2qI_{dark}G_{det}^2F + 2qI_{dc}\right)B_{en}}}{SG_{det}}, \tag{13}$$

where P_{bg} is the optical solar background noise, P_{sig} is the optical power of the signal, I_{dark} is optical dark current, I_{dc} is the DC dark current, G_{det} is the detector current gain, B_{en} is effective noise bandwidth ($= \frac{\pi B}{2}$), S is radiant sensitivity of the detector (amp/watt), F

is excess noise factor which is equal to 1 for photodiode, and q is the electronic charge. The total NEP is given by

$$N_T = \sqrt{P_{bg\_sn}^2 + P_{sig\_sn}^2 + P_{dark\_sn}^2}. \tag{14}$$

To design a short-range FSOC system using laser as transmitter, all the noise contributions need to be incorporated in calculation. As the bit-rate requirement is increasing day-by-day, receiver components and circuit are required to be very sensitive and responsive. With the increase of sensitivity, receiver noise budget is becoming smaller.

By using the residual SI model of [22,23], residual SI power at nodes A and B are given by $\Gamma_{sA} = \frac{P_A^{1-\delta}}{\beta\mu^\delta}$ and $\Gamma_{sB} = \frac{P_B^{1-\delta}}{\beta\mu^\delta}$, where β represents the coefficient of SI suppression by separation of the transmitter and the receiver within the same transceiver unit, and μ and δ represent SI suppression parameters for deployed passive SI cancellation technique. P_A and P_B are the transmitted signal power at nodes A and B, respectively.

4.2. Optimized SINR formulation

SINR characterizes the quality of a communication system as well as it is the performance parameter for a transceiver. Considering an FSO link established using transceivers A and B, each with a single transmitter having a divergence angle of θ and a single receiver having a detection area of A_{det}, SINR can be written for node A as [21]

$$SINR_A = \left[\frac{P_B L_z(d,\lambda) A_{det}\cos(\phi \pm \delta)}{(\tan\theta)^2 4d^2(N_T + \Gamma_{SA})}\right]^2, \tag{15}$$

where P_B is the transmit power at node B, d is the link distance, and $L_z(d,\lambda)$ is the free-space loss parameter for a link distance of d. The expressions of L_z, N_T, and Γ_{SA} are shown in Sections 3 and 4.1 . ϕ is the pointing error angle when the transceivers are perfectly aligned, and δ is the 'vibration angle' which is the additional pointing error due to vibration on the mobile transceivers.

For a multi-element FSO transceiver with N transmitters having θ divergence angle each and m receivers with detection area of A_{det}, SINR for node A can be expressed as

$$SINR_A = \sum_{i=1}^{N} \sum_{j:j\in\mathcal{F}_i} \left[\frac{P_{B,i} L_z(d,\lambda) A_{det}\cos(\phi_j \pm \delta_j)}{(\tan\theta)^2 4d^2(N_T + \Gamma_{SA})}\right]^2, \tag{16}$$

where i and j denote the index of transmitter and receiver, respectively. $P_{B,i}$ denotes the transmit power at transmitter i at node B. Each transmit beam projects a beam footprint on the transceiver plane and only covers a subset of the available receivers in a transceiver. $\mathcal{F}_i$ represents the set of receivers that falls within the beam footprint of transmitter i. ϕ_j and δ_j are the pointing error and the vibration angles on the beam arriving at receiver $j \in \mathcal{F}_i$.

To maximize SINR, we need to find the optimum number of transmitters N and receivers m, as well as the positions, $p_i(x_i, y_i)$, of the transmitters on the transceiver plane. By choosing the best transmitter positions we can find the best tiling patterns of the transceivers. For the sake of uniformity, we will consider identical tiling at both transceiver nodes A and B, same divergence angle θ for all transmitters, and same transmit power P_B for all transmitters. So, the optimization problem becomes

$$\begin{aligned} \max_{N,\ p_i} \quad & SINR_A \\ \text{s.t.} \quad & N < N_m, \\ & A_T = N A_{trans} + m A_{det}, \end{aligned} \tag{17}$$

where A_{trans} is the area of each transmitter occupied in the transceiver plane and N_m is the maximum number of transmitters that can be placed on the transceiver plane. We do not include m as a parameter of the optimization since we assume that for all the positions where a transmitter is not placed, a receiver is placed, i.e., $N_m = N + m$.

Each transmitter i projects a Gaussian beam footprint on the receiver plane centered at the corresponding location of transmitter i with a diameter of $d\tan\theta$. $\mathcal{F}_i$ consists of m_i' receivers that falls within the beam footprint. So, the SINR of the IBFD FSO link at node B under no vibration can be written as

$$SINR_A = \sum_{i=1}^{N} \Pi_i, \tag{18}$$

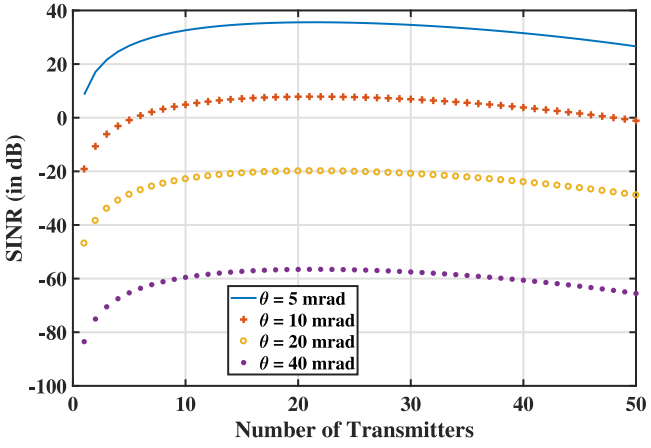

Fig. 5. SINR calculation for different divergence angles of the transmitters, while $d = 100$ m, $\phi = 3.4$ mrad, and $P_T = 10$ mW.

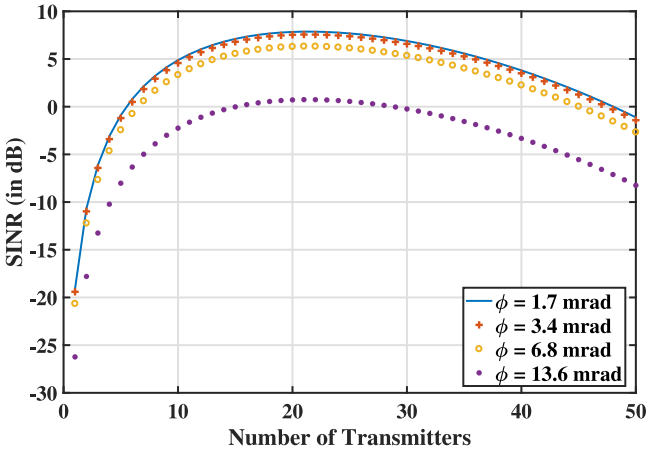

Fig. 6. SINR calculation different positioning of transmitters in the transceiver plane, while $d = 100$ m, $\theta = 10$ mrad, and $P_T = 10$ mW.

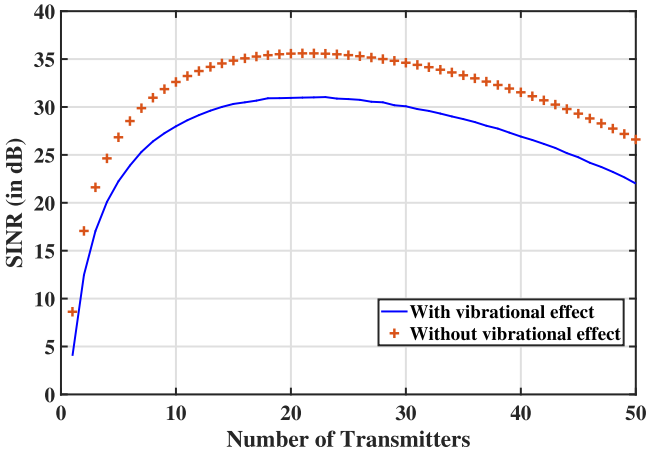

Fig. 7. Effect on SINR at the presence of vibration of the mobile platform for $d = 100$ m, $\phi = 1.7$ mrad, $\theta = 5$ mrad, and $P_T = 10$ mW.

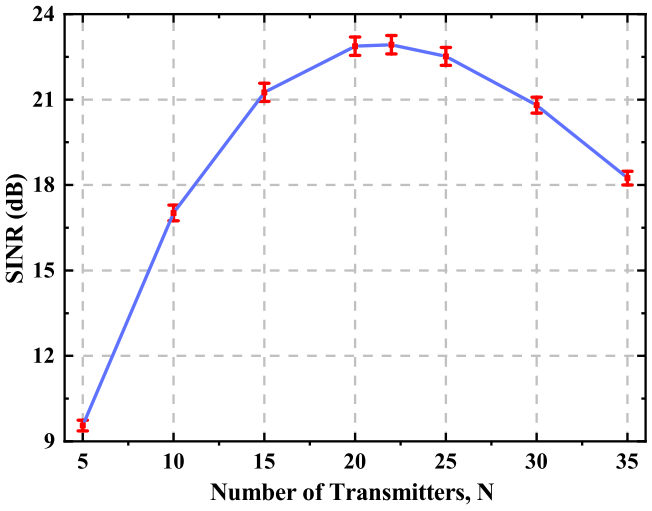

Fig. 8. Variation of SINR when transmitters with $\theta = 5$ mrad divergence angle are placed randomly on 10 × 10 transceiver grid, while $d = 50$ m and $P_T = 10$ mW.

where

$$\Pi_i = \sum_{j:j\in\mathcal{F}_i} \left[\frac{P_B L_z(d,\lambda) A_{det}\cos(\phi_j)}{(\tan\theta)^2 4d^2 (N_T + \Gamma_{SA})}\right]^2. \tag{19}$$

We find the optimum transmitter count, N^*, maximizing $SINR_A$ by calculating $\frac{\partial}{\partial N}(SINR_A) = 0$. Using Eq. (18) we get

$$\begin{aligned}\frac{\partial}{\partial N}(SINR_A) &= \frac{\partial}{\partial N}\sum_{i=1}^{N}\Pi_i \\ &= \frac{\partial}{\partial N}(\Pi_1 + \Pi_2 + \cdots + \Pi_N).\end{aligned} \tag{20}$$

Each term of Π_i on the right hand side of Eq. (20) largely depends on the relative location of the transmitter i, as that determines how many receivers (m_i') are covered by the beam footprint. Increase of transmitters also means reduction of receivers, essentially resulting in reduced receiver area to capture the beam signal. So, the ratio of the total receiver area to the total transceiver area is another parameter that can be used to optimize $SINR$. In order to attain an analytical solution to N^*, we consider the case when this ratio is fixed, i.e., m_i' is constant regardless of i. This case happens when the link distance (d) is long and/or the divergence angle (θ) of the transmitters is large. In particular, this case would happen when the radius of the beam footprint is greater than or equal to the diagonal of the transceiver plane. Assuming that both transmitters and receivers are square-shaped and are the same in size (i.e., the receiver and the transmitter areas are both equal to A_{det}), this case would happen when $d\tan\theta \geq \sqrt{2N_m A_{det}}$. Then, $\mathcal{F}_i$ consists of all the available receivers on the transceiver which yields $m_i' = N_m - N$, and Eq. (19) becomes

$$\Pi_i = \sum_{j=1}^{N_m - N} \chi_i \left(1 - \frac{\phi_j^2}{2}\right)^2, \tag{21}$$

where $\chi_i = \left[\frac{P_B L_z(d,\lambda) A_{det}}{(\tan\theta)^2 4d^2 (N_T+\Gamma_{SA})}\right]^2$, and $\cos(\phi_j)$ is approximated with the first two terms of Taylor expansion. Now, each receiver has pointing error angle with respect to each transmitter. If the transmitters and receivers are uniformly distributed, the pointing error angle can be approximated by $\phi_j = j\phi$, where ϕ is the minimum pointing error angle. Then, Eq. (21) can be written as

$$\Pi_i = \chi_i\left[(N_m - N) - \phi^2\frac{(N_m - N)(N_m - N + 1)(2N_m - 2N + 1)}{6}\right]. \tag{22}$$

As we assumed every transmitter's beam footprint is covering the whole transceiver area, each Π_i becomes identical. By using the expression from Eq. (22), Eq. (18) can be written as

$$\begin{aligned}SINR_A = \chi N\Big[&(N_m - N) - \frac{\phi^2}{3}N_m^3 + \phi^2 N_m^2 N \\ &- \phi^2 N_m N^2 + \frac{\phi^2}{3}N^3 - \frac{\phi^2}{2}N_m^2 + \phi^2 N_m N \\ &- \frac{\phi^2}{2}N^2 - \frac{\phi^2}{6}N_m - \frac{\phi^2}{6}N\Big].\end{aligned} \tag{23}$$

By differentiating the term from Eq. (23), we get

$$\begin{aligned}\frac{\partial}{\partial N}(SINR_A) = \chi\Big[&N_m - 4N + 2\phi^2 N_m^2 N - 3\phi^2 N_m N^2 \\ &+ \frac{4}{3}\phi^2 N^3 + 2\phi^2 N_m N - 3\frac{\phi^2}{2}N^2 - \frac{\phi^2}{3}N \\ &- \frac{\phi^2}{3}N_m^3 - \frac{\phi^2}{2}N_m^2 - \frac{\phi^2}{6}N_m\Big].\end{aligned} \tag{24}$$

By simplifying the equation and setting $\frac{\partial}{\partial N}(SINR_A) = 0$, we get

$$aN^3 + bN^2 + cN + d = 0, \tag{25}$$

where

$$\begin{aligned}a &= \frac{4}{3}\phi^2, \\ b &= -\frac{\phi^2}{2} - 3\phi^2 N_m, \\ c &= 2\phi^2 N_m^2 + 2\phi^2 N_m - 4 - \frac{\phi^2}{3}, \\ d &= N_m - \frac{\phi^2}{6}N_m - \frac{\phi^2}{2}N_m^2 - \frac{\phi^2}{3}N_m^3.\end{aligned}$$

Now, the value of N_m can range from few tens to few hundreds and ϕ is in the order of mrad for practical cases. In that case, the coefficients approximated as $a \approx 0$, $b \approx 0$, $c \approx -4$, and $d \approx N_m$. The optimum number of transmitter reduces to $\frac{N}{N_m} \approx 0.25$. This solution represents the case when pointing error angles are negligible. However for practical cases, due to finite pointing error angles the optimum solution for N^* is smaller than $0.25N_m$.

In the following section, we implemented a numerical solution of the optimization problem by using randomly generated sets. First we calculated the optimum number of transmitters (N) and then the optimum positions (p_i) of the transmitters on the transceiver plane. We also implemented a genetic evolution algorithm technique to find the optimum positions of the transmitters.

5. Approach one: Randomly generated sets

To determine the optimum tiling positions of the transceiver elements, we developed a MATLAB tool to simulate the communication link and calculate $SINR$ for each node. For this simulation, we used 50 m long FSO channel between two UAVs communicating in IBFD mode using wavelength $\lambda = 900$ nm. The transceiver size is set to 10 cm × 10 cm. We assume that direct LOS is already established, however the vibrational effects from the UAVs is still present which can lead to pointing error of the link.

As the position of each transmitter is varied on the transceiver plane, a pointing error with the other node takes place. This pointing error is calculated in terms of pointing angle, ϕ. On top of this angular pointing error ϕ, vibration of the mobile platform incorporates additional error, which is also calculated in terms of angular error ($\pm\delta$). These pointing angle errors are shown in Fig. 3. Fig. 4 shows two categories of possible tiling schemes. In one scheme, all the transmitters are positioned equidistant from the center of the transceiver plane. On the other hand, all transmitters are positioned randomly in the second scheme. In this case, we randomly selected N transmitter slots and the rest are considered to be receiver area. Free-space path loss is calculated for determining $SINR$ for our channel, which is shown in Fig. 2.

To determine the number of the transmitters required to obtain the best performance, we simulated the FSO link by varying the transmitter

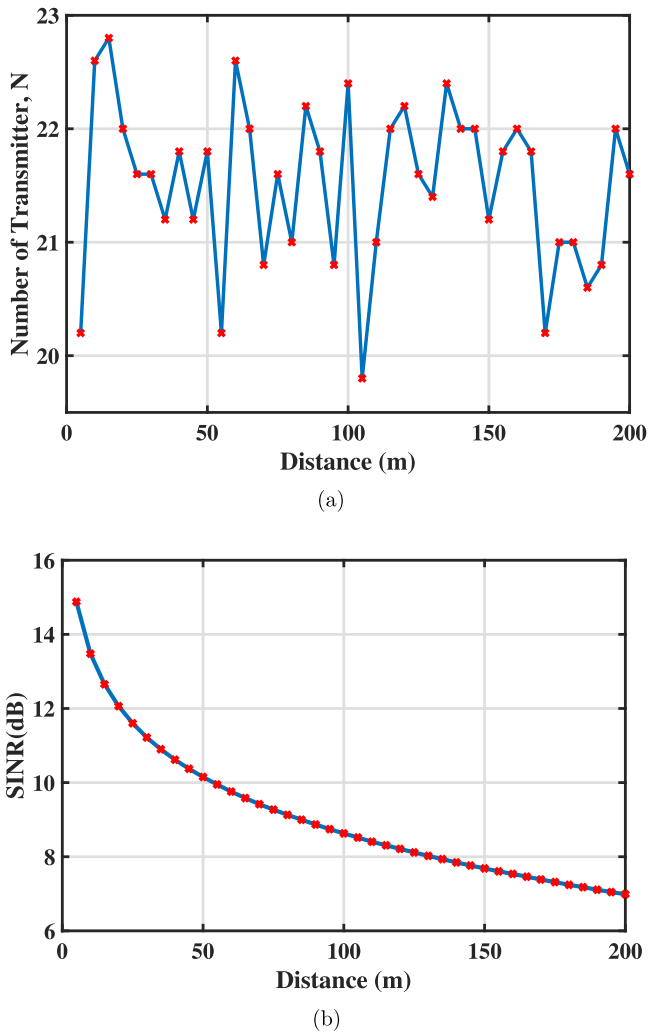

Fig. 9. (a) Optimum number of transmitter (N) and (b) SINR variation for different link range (d).

count from 1 to 99, out of possible 100 positions, and calculated $SINR$ for different divergence angles (θ). We can observe from Fig. 5 that best performance of the link occurs when number of transmitters (N) is 22, irrespective of divergence angles. With the increase of the transmitter count, receiver area reduces and that results into degraded link performance. Also, by increasing divergence angle, most of the power collected at the receiver end also reduces, and we can observe the reduction of $SINR$.

We investigated further by varying the position of the transmitters on the transceiver plane and hence changing the pointing error angle (ϕ) by using equidistant scheme from Fig. 4. Fig. 6 shows the results for different ϕ values and calculated by varying N. We can again observe that the best case performance can be achieved for $N = 22$. Fig. 7 shows the effect of vibration on the link performance of the FSO channel. Fig. 8 shows the average and standard deviation of the calculated $SINR$ for different N values. We also randomly generated vibrations and repeated the simulation for 1000 times to incorporate the effects of vibration into the simulation. Even though the overall $SINR$ obtained is reduced by introducing vibration, best case scenario still occurs at $N = 22$, or we can say 22% area of the transceiver plane needs to covered with transmitters. Even when the link distance is varied over a large range, the optimum number of transmitters remains close to 22%, whereas average SINR drops exponentially with distance as shown in Fig. 9. By using the simulation parameters and solving the equation derived in Eq. (25), we get $N = 25$. The analytical solution was an approximation of the real-world scenario, however we got fairly close solutions.

We incorporated all the findings we gathered from the simulations of equidistant scheme into the random position scheme as shown in Fig. 4. We increased the grid size of the transceiver plane to 100×100 array. We generated 100,000 sets of transceiver planes with randomly positioned transmitters for each N, in this case, to cover 22% area of the plane, we set $N = 2200$. To determine the optimum positions of the transmitters for $N = 2200$, we selected best 1,000 sets out of randomly generated 100,000 sets based on $SINR$ performance. We repeated the process for 3 times with seed values. Finally, we constructed a heatmap of the transceiver plane by overlapping the best tiling sets (more dark means more transmitters were placed at that position in these tiling sets) in Fig. 10(a) at the presence of vibrational effects. We can observe from the figure that the best performance can be achieved when majority of the transmitters are positioned around the center of the plane, with receiving areas at the center. The reason for the disperse positioning due to the presence vibrational effects of the mounting platform is the Gaussian beam profile of the transmit signal and the beam centers carry most of the energy. If the transmitters are positioned around the edges, the center of the beams might fall outside of the transceiver plane and most of the energy goes undetected at the presence of vibration. To accommodate for such cases, the optimum transmitter positions are clustered in four separate areas located mid-way from the center to the corners of the transceiver plane so that at least the center of the beams from those 'edge transmitters' could fall on the receiving plane.

It is notable that the center of the transceiver plane does include only few receivers instead of being entirely covered with transmitters. The intuition behind this is that the center of the optical beam carries most of the energy. If the center of the plane is covered entirely by transmitters, the center of the beams coming from the other plane would not be received and only the outer part of those beams would be received, resulting in a small aggregate received intensity. With the presence of vibration, however, the best transmitter positions are more dispersed to increase the likelihood of receiving the center of the beams coming from the other side.

This random set based technique of obtaining the optimum solution is computationally heavy and as we checked only a fraction of the available solutions due to limitation of computational capacity and time, hence a more efficient method is required. To overcome this computational complexity, we next devise a heuristic optimization method based on genetic algorithms.

6. Approach two: Genetic algorithm

In order to tackle the computational complexity of the randomized set selection and to find solutions closer to the optimum, we devise a genetic algorithm approach to the problem of tiling positions of the transmitters on the transceiver plane. As the transceiver plane is divided into a 100×100 grid, it gives us in total 10,000 different position to consider for transmitters. Essentially the size of the search space for the optimization problem becomes $2^{10000} - 1$. Using the randomly generated sets to determine the optimum tiling will require huge computational time. Even in the optimization approach presented in the previous section, we only explored a fraction of the every possible tiling combination. Genetic algorithm gives a faster way to approach the optimum and it also requires smaller computational capacity.

To implement the genetic algorithm, we start with fewer number of randomly generated sets of the transceiver plane. To reduce the complexity of the problem, we consider 22% of the area is covered with transmitters, as we determined in the previous section. To start the process, we randomly generate 5,000 different sets and calculate SINR for each set. We determine the best 10% sets out of the total population based on $SINR$ calculation, which we can call the 'fit population'. We

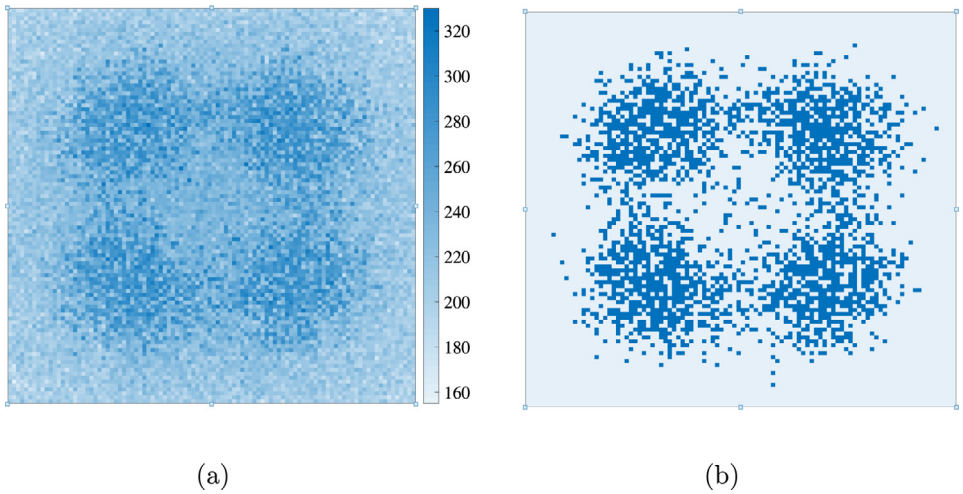

Fig. 10. (a) Heatmap of transmitter locations on a 100 × 100 transceiver grid for best performances out of randomly generated set, (b) Transmitter locations based on the heatmap generated from best performing sets.

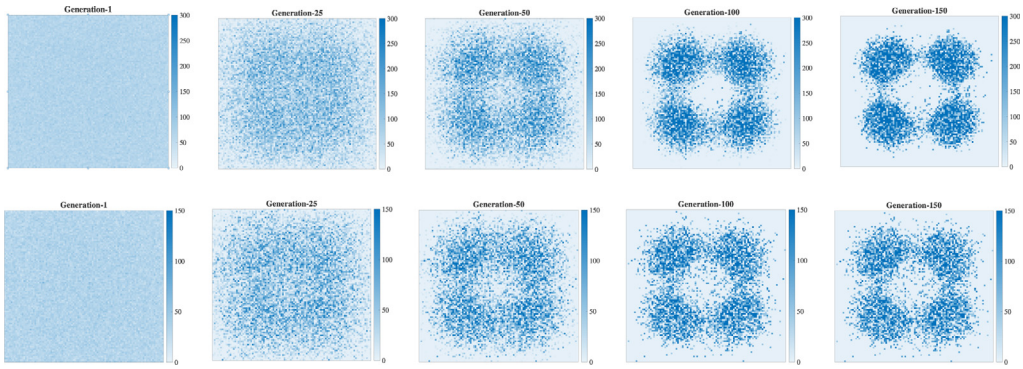

Fig. 11. Heatmap of transmitter locations on a 100 × 100 transceiver grid for best performances for different generations of genetic evolution, Top Row: 20% fit population, Bottom Row: 10% fit population.

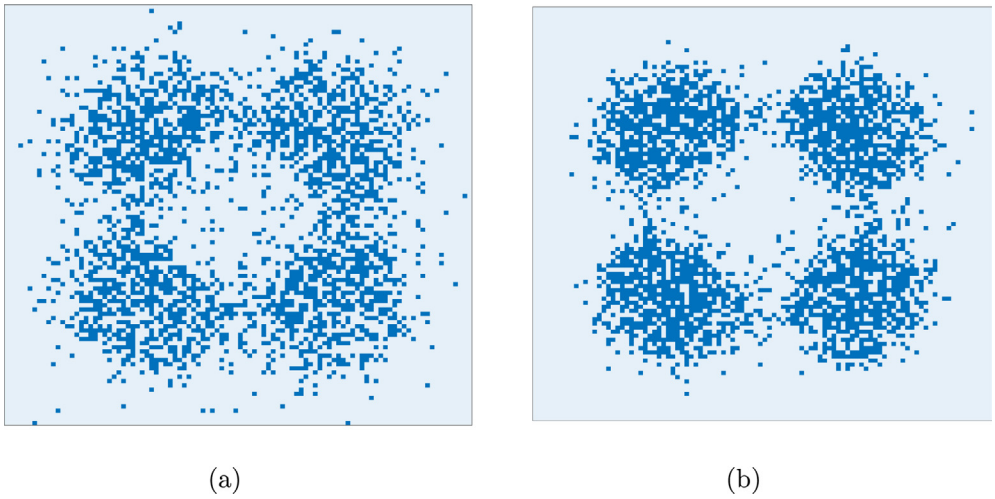

Fig. 12. Optimized transmitter locations on a 100 × 100 transceiver grid (a) using genetic evolution after generation 150 with 10% fit population with vibrational effect, (b) using genetic evolution after generation 150 with 20% fit population with vibrational effect.

use the 'fit population' to generate the next generation by applying crossover technique. We randomly select two members from the current fit population to obtain a member of the next generation. The crossover is done over two steps: first, we identify the common positions of the two selected parents and we retain the common positions in the child. Second, we select rest of the transmitter positions from each parent in $1:1$ ratio. We repeat the process to obtain the entire population for the next generation and calculate SINR for each set. The process is repeated until we do not see any significant improvement in the average $SINR$ value of the fit population for three (3) consecutive generations or a certain number of generations are obtained. A pseudo-code of the algorithm is presented in Algorithm 1.

Algorithm 1 Genetic Algorithm for Optimized Tiling

```
Initialize Transmitter count, N
Initialize Transceiver plane
Initialize Population Set count, P
Set ϵ as SINR tolerance
flag=TRUE
Generate Population Set by random selection for Generation 1
Calculate SINR for each set
while flag is TRUE do
    Identify Best f% as fit population seed for Generation i + 1
    Generate Population Set by crossover() for Generation i + 1
    Calculate SINR for each set
    Compare SINR with Generation i
    if SINR(i+1)−SINR(i)< ϵ for 3 consecutive generations then
        flag=FALSE
    else
        repeat next generation
    end if
end while
```

crossover()

```
Choose two (2) parents randomly from the fit population
Determine common transmitter positions for the parents
Keep common transmitter positions for the child
Choose rest of the transmitter positions from both parents randomly at 1:1 ratio
```

We presented the evolution of the optimized tiling solutions over different generations in Fig. 11. The heatmaps are generated by overlapping the transmitter tiling positions of the members of the fit populations of each generation. We can observe from the figures that transmitters around the center with receiving area at the center gives best performance, as we observed from the randomly generated sets in the previous section. Hence, the convergence over the generations are observed as the transmitter locations are more clustered in four lobes located midway towards the corners of the transceiver plane from the center. We also changed the fit population size to 10% and observed the similar convergence pattern as well. After about 50 generations, both 20% and 10% fit population cases indicates most of the transmitters should be positioned around the center of the panel, as we have observed from the randomly generated sets. As vibrational effect tends to introduce higher combined pointing error angle, transmitters being around the center makes it more convenient for the receiving end to capture most of the energy even at the presence of vibrations using this tiling pattern. Later, we determine the best positions of the transmitter positions after 150 generations and shown in Fig. 12(a) and 12(b). Both of these tiling solutions indicates optimum transmitter positions to obtain best $SINR$ performance under vibrational effects. Comparing the solutions of the genetic algorithm with the solution from randomly generated cases shown in Fig. 10(b), we establish that we can obtain the optimized tiling solution using the genetic algorithm approach utilizing much smaller computational capability.

To understand the effect of the genetic algorithm parameters on the results, we varied the fit population size and observed $SINR$ over generations. To determine how many generations it requires to achieve the $SINR$ saturation, we vary the fit population size for different values from 20% to 1%. All every cases, total population size of a generation was fixed at 5,000 and number of transmitters, $N = 2200$. Fig. 13 shows variation of the peak $SINR$ of the fit populations over generations. As shown in Fig. 13, smaller fit population yields better solutions in early generations but converges to a more sub-optimal solution eventually. However, we can achieve best $SINR$ performance when the fit population is increased. Essentially this requires generating more generations and computational time. We summarized the results from the genetic algorithm simulations in Table 1. In both Fig. 13, we inserted a gray solid line that indicated the value from randomly generated sets. We can clearly observe genetic algorithm approach consistently outperforms the randomized set selection after about 20 generations.

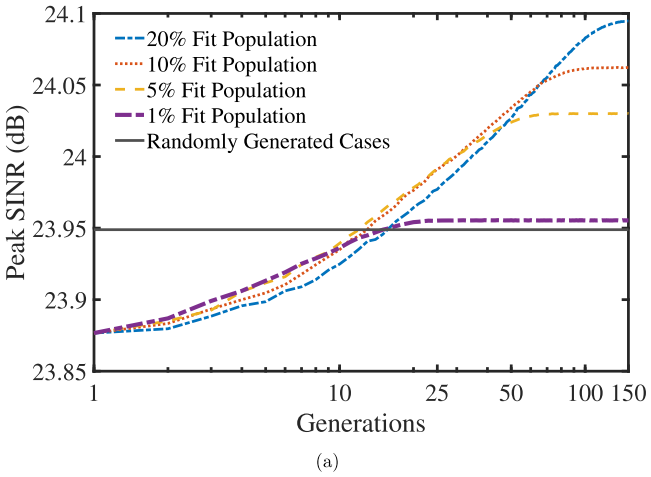

Fig. 13. Peak SINR of the fit population over 150 generations of evolution.

Table 1
Summary of genetic algorithm simulations.

Fit Population size	# of Generations to Converge	Peak SINR (dB)
20%	190	24.09
10%	145	24.06
5%	100	24.03
1%	80	23.96

7. Conclusion

In conclusion, we have outlined a model for optimizing the tiling position for multi-element transceiver design. We have incorporated weather effect and SI that arise within a transceiver unit to obtain a design model for simulating in-band full-duplex FSO channel. A simulation tool is developed in MATLAB to determine the best performance for optimizing communication throughput even under the presence of vibrational effect of the mobile platform. We presented that for a transceiver plane consisting 10×10 grid size, the best performance can be achieved for $N = 22$. Later, we extended that tiling technique to 100×100 grid with 22% area covered by transmitters. We explored randomly generated sets to explore the optimum solution, however, complexity of the problem makes it difficult to reach optimum solution. We also implemented a Genetic Algorithm technique to optimize the tiling positions. We presented a guideline for positioning the transmitters within transceiver plane using both approaches. The model can be further improved by including sway and tilt of the transceiver platform and by considering multi-channel link design where inter-symbol interference plays additional role on the performance of the aggregated link. Also, optimizing transmit power (P_i) for each transmitter and dynamic optimization of transmitter count (N^*) during genetic algorithm can be investigated as future study.

Declaration of competing interest

The authors declare the following financial interests/personal relationships which may be considered as potential competing interests: This work was supported in part by National Science Foundation awards 1836741, 1647189, and 2006683.

Acknowledgments

This work was supported in part by U.S. National Science Foundation (NSF) award 1836741.

References

[1] M. Khan, M. Yuksel, G. Winkelmaier, GPS-free maintenance of a free-space-optical link between two autonomous mobiles, IEEE Trans. Mob. Comput. 16 (6) (2017) 1644–1657.

[2] M. Khan, M. Yuksel, Autonomous alignment of free-space-optical links between UAVs, in: Proceedings of the 2nd International Workshop on Hot Topics in Wireless, ACM, 2015, pp. 36–40.

[3] C.W.J. Oh, Z. Cao, E. Tangdiongga, T. Koonen, 10 Gbps all-optical full-duplex indoor optical wireless communication with wavelength reuse, in: OFC, Optical Society of America, 2016, pp. Th4A–6.

[4] X. Xie, X. Zhang, Does full-duplex double the capacity of wireless networks? in: INFOCOM, IEEE, 2014.

[5] S. Goyal, P. Liu, O. Gurbuz, E. Erkip, S. Panwar, A distributed MAC protocol for full duplex radio, in: Signals, Systems and Computers, 2013 Asilomar Conference on, IEEE, 2013, pp. 788–792.

[6] Z. Zhang, B. Li, Neighbor discovery in mobile ad hoc self-configuring networks with directional antennas: Algorithms and comparisons, IEEE Trans. Wireless Commun. 7 (5) (2008).

[7] K. Wang, A. Nirmalathas, C. Lim, K. Alameh, E. Skafidas, Full-duplex gigabit indoor optical wireless communication system with CAP modulation, Photonics Tech. Lett. 28 (7) (2016) 790–793.

[8] Y. Wang, Y. Wang, N. Chi, J. Yu, H. Shang, Demonstration of 575-Mb/s downlink and 225-Mb/s uplink bi-directional SCM-WDM visible light communication using RGB LED and phosphor-based LED, Opt. Express 21 (1) (2013) 1203–1208.

[9] B.E. Johnson, T.A. Lindsay, D.L. Brodeur, R.E. Morton, M.A. Regnier, Wide-angle, high-speed, free-space optical communications system, US Patent 5,359,446, 1994.

[10] A.F.M.S. Haq, M.R. Khan, M. Yuksel, A prototype of in-band full-duplex free-space optical transceiver, in: 2018 IEEE International Symposium on Local and Metropolitan Area Networks (LANMAN), IEEE, 2018, pp. 112–113.

[11] A.F.M.S. Haq, M. Khan, M. Yuksel, Asynchronous LOS discovery algorithm for aerial nodes using in-band full-duplex transceivers, in: Proceedings of the 15th International CoNEXT, ACM, 2019.

[12] J. Akella, M. Yuksel, S. Kalyanaraman, Multi-element array antennas for free-space optical communication, in: Second IFIP International Conference on Wireless and Optical Communications Networks, 2005. WOCN 2005, IEEE, 2005, pp. 159–163.

[13] M. Bilgi, M. Yuksel, Multi-element free-space-optical spherical structures with intermittent connectivity patterns, in: IEEE INFOCOM Workshops 2008, IEEE, 2008, pp. 1–4.

[14] A. Kaadan, H.H. Refai, P.G. LoPresti, Multielement FSO transceivers alignment for inter-UAV communications, J. Lightwave Technol. 32 (24) (2014) 4785–4795.

[15] Y.S. Eroğlu, I. Güvenç, A. Şahin, Y. Yapıcı, N. Pala, M. Yuksel, Multi-element VLC networks: LED assignment, power control, and optimum combining, IEEE J. Sel. Areas Commun. 36 (1) (2017) 121–135.

[16] S.I. Mushfique, A. Alsharoa, M. Yuksel, Optimization of SINR and illumination uniformity in multi-LED multi-datastream VLC networks, IEEE Trans. Cogn. Commun. Netw. (2020).

[17] H. Weichel, Laser Beam Propagation in the Atmosphere, Vol. 3, SPIE Press, 1990.

[18] H. Manor, S. Arnon, Performance of an optical wireless communication system as a function of wavelength, Appl. Opt. 42 (21) (2003) 4285–4294.

[19] I.I. Kim, B. McArthur, E.J. Korevaar, Comparison of laser beam propagation at 785 nm and 1550 nm in fog and haze for optical wireless communications, in: Optical Wireless Communications III, Vol. 4214, International Society for Optics and Photonics, 2001, pp. 26–38.

[20] A.A. Farid, S. Hranilovic, Outage capacity optimization for free-space optical links with pointing errors, J. Lightwave Technol. 25 (7) (2007) 1702–1710.

[21] J.W. Giles, I.N. Bankman, Underwater optical communications systems. Part 2: Basic design considerations, in: MILCOM 2005-2005 IEEE Military Comm. Conf., IEEE, 2005, pp. 1700–1705.

[22] M. Duarte, C. Dick, A. Sabharwal, Experiment-driven characterization of full-duplex wireless systems, IEEE Trans. Wireless Commun. 11 (12) (2012) 4296–4307.

[23] A.F.M.S. Haq, M. Yuksel, Weather-limited in-band full-duplex transceiver model for free-space optical communication, Opt. Eng. 59 (5) (2020) 056113.